



Self-Masked Aldehyde Inhibitors of Human Cathepsin L Are Potent Anti-CoV-2 Agents

Jiyun Zhu¹, Linfeng Li^{1±}, Aleksandra Drelich², Bala C. Chenna¹, Drake M. Mellott^{1±}, Zane W. Taylor^{3±}, Vivian Tat², Christopher Z. Garcia¹, Ardala Katzfuss¹, Chien-Te K. Tseng² and Thomas D. Meek^{1*}

OPEN ACCESS

Edited by:

Matthew Bogyo,
Stanford University, United States

Reviewed by:

Nicola Micale,
University of Messina, Italy
Reik Löser,
Helmholtz Association of German
Research Centres (HZ), Germany

*Correspondence:

Thomas D. Meek
Thomas.Meek@ag.tamu.edu

*Present Address:

Linfeng Li,
Center for Novel Target and
Therapeutic Intervention, Institute of
Life Sciences, Chongqing Medical
University, Chongqing, China
Drake M. Mellott, Agios Pharmaceuticals,
Cambridge, MA, United States
Zane W. Taylor, RD Platform Technology
and Science, GlaxoSmithKline
Pharmaceuticals, Collegeville, PA,
United States

Specialty section:

This article was submitted to
Chemical Biology,
a section of the journal
Frontiers in Chemistry

Received: 01 February 2022

Accepted: 12 April 2022

Published: 04 July 2022

Citation:

Zhu J, Li L, Drelich A, Chenna BC,
Mellott DM, Taylor ZW, Tat V,
Garcia CZ, Katzfuss A,
Tseng C-T and Meek TD (2022) Self-
Masked Aldehyde Inhibitors of Human
Cathepsin L Are Potent Anti-CoV-
2 Agents.
Front. Chem. 10:867928.
doi: 10.3389/fchem.2022.867928

¹Department of Biochemistry and Biophysics, College of Agriculture and Life Sciences, Texas A&M University College Station, College Station, TX, United States, ²Department of Microbiology and Immunology, John Sealy School of Medicine, University of Texas Medical Branch at Galveston, Galveston, TX, United States, ³Department of Chemistry, College of Science, Texas A&M University College Station, College Station, TX, United States

Cysteine proteases comprise an important class of drug targets, especially for infectious diseases such as Chagas disease (cruzain) and COVID-19 (3CL protease, cathepsin L). Peptide aldehydes have proven to be potent inhibitors for all of these proteases. However, the intrinsic, high electrophilicity of the aldehyde group is associated with safety concerns and metabolic instability, limiting the use of aldehyde inhibitors as drugs. We have developed a novel class of compounds, self-masked aldehyde inhibitors (SMAs) which are based on the dipeptide aldehyde inhibitor (Cbz-Phe-Phe-CHO, **1**), for which the P₁ Phe group contains a 1'-hydroxy group, effectively, an *o*-tyrosinyl aldehyde (Cbz-Phe-*o*-Tyr-CHO, **2**; (Li *et al.* (2021) *J. Med. Chem.* 64, 11,267–11,287)). Compound **2** and other SMAs exist in aqueous mixtures as stable δ -lactols, and apparent catalysis by the cysteine protease cruzain, the major cysteine protease of *Trypanosoma cruzi*, results in the opening of the lactol ring to afford the aldehydes which then form reversible thiohemiacetals with the enzyme. These SMAs are also potent, time-dependent inhibitors of human cathepsin L (K_i = 11–60 nM), an enzyme which shares 36% amino acid identity with cruzain. As inactivators of cathepsin L have recently been shown to be potent anti-SARS-CoV-2 agents in infected mammalian cells (Mellott *et al.* (2021) *ACS Chem. Biol.* 16, 642–650), we evaluated SMAs in VeroE6 and A549/ACE2 cells infected with SARS-CoV-2. These SMAs demonstrated potent anti-SARS-CoV-2 activity with values of EC_{50} = 2–8 μ M. We also synthesized pro-drug forms of the SMAs in which the hydroxyl groups of the lactols were O-acylated. Such pro-drug SMAs resulted in significantly enhanced anti-SARS-CoV-2 activity (EC_{50} = 0.3–0.6 μ M), demonstrating that the O-acylated-SMAs afforded a level of stability within infected cells, and are likely converted to SMAs by the action of cellular esterases. Lastly, we prepared and characterized an SMA in which the sidechain adjacent to the terminal aldehyde is a 2-pyridonyl-alanine group, a mimic of both phenylalanine and glutamine. This compound (**9**) inhibited both cathepsin L and 3CL

Abbreviations: AMC, 7-amino-4-methylcoumarin; CHAPS, 3-[3-(cholamidopropyl)dimethylammonio]-1-propanesulfonate; Cbz/Z, benzyloxycarbonyl; DMSO, dimethyl sulfoxide; DTT, dithiothreitol; EDTA, ethylenediaminetetraacetic acid; SMAI, self-masked aldehyde inhibitor; Z-FR-AMC, carboxybenzyl-L-phenylalanine-L-arginine-7-amino-4-methylcoumarin.

protease at low nanomolar concentrations, and also exerted anti-CoV-2 activity in an infected human cell line.

Keywords: SARS coronavirus-2, cathepsin L, self-masked aldehydes, reversible covalent inactivation, COVID-19, cysteine proteases

INTRODUCTION

The global COVID-19 pandemic, caused by the β -coronavirus SARS-CoV-2, has, as of the end of 2021, resulted in 289 million cases and 5.4 million deaths worldwide (Johns Hopkins University of Medicine, 2022). The socio-economic consequences of this pandemic are difficult to overstate. Despite the availability of effective vaccines since 2021, and the recent (emergency use) approval of a bespoke, small-molecule drug (Paxlovid (Pfizer, 2021); nirmatrelvir, combined with ritonavir) for the treatment of COVID-19, the emergence of new variant forms of the SARS-CoV-2 virus, such as the delta and omicron strains, will require further discovery of new therapeutic agents to counter the inevitable development of SARS-CoV-2 variants that are resistant to these first-generation drugs.

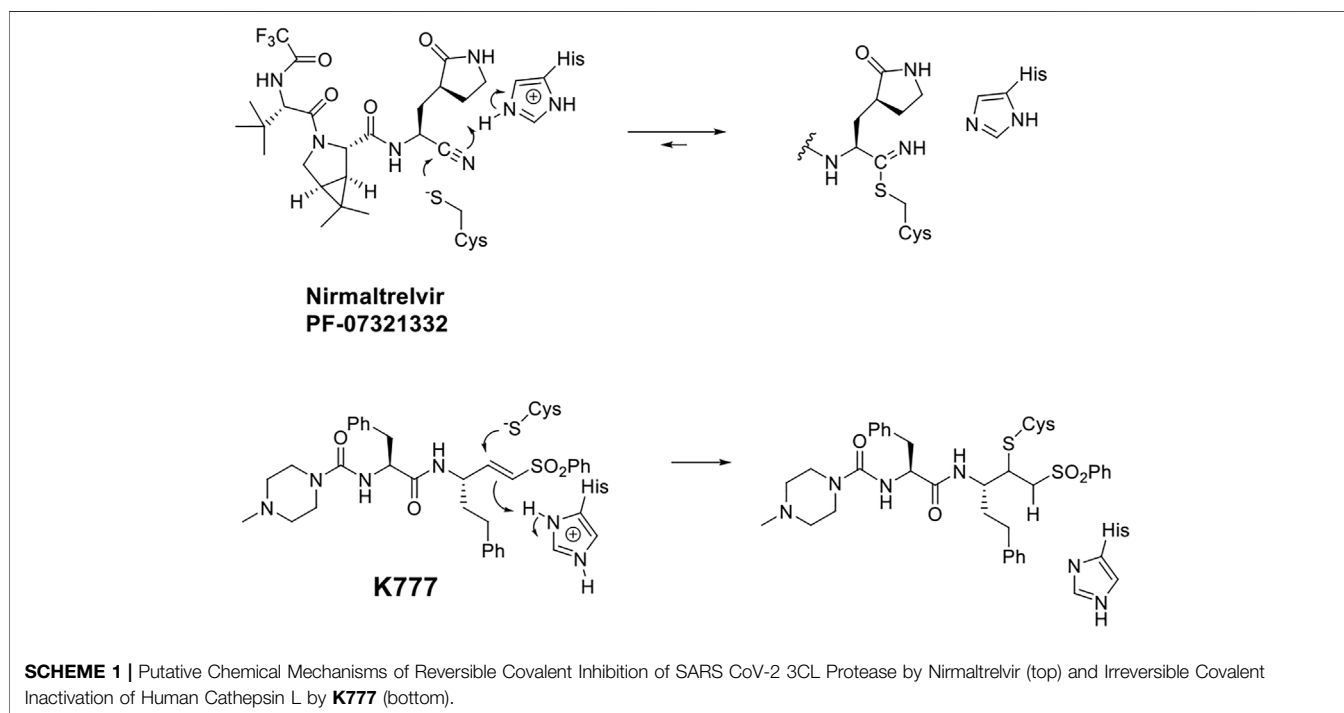
The virally-encoded cysteine protease known as the Main protease, or 3CL protease (Zhang et al., 2020; Dai et al., 2020; and Mellott et al., 2021), is the target of nirmatrelvir, also known as **PF-07321332** (Owen et al., 2021) (**Scheme 1**). **PF-07321332** exerts reversible covalent inhibition of the 3CL protease by a putative mechanism of action involving the formation of a thioimidate adduct (**Scheme 1**) (Bai et al., 2021; Owen et al., 2021).

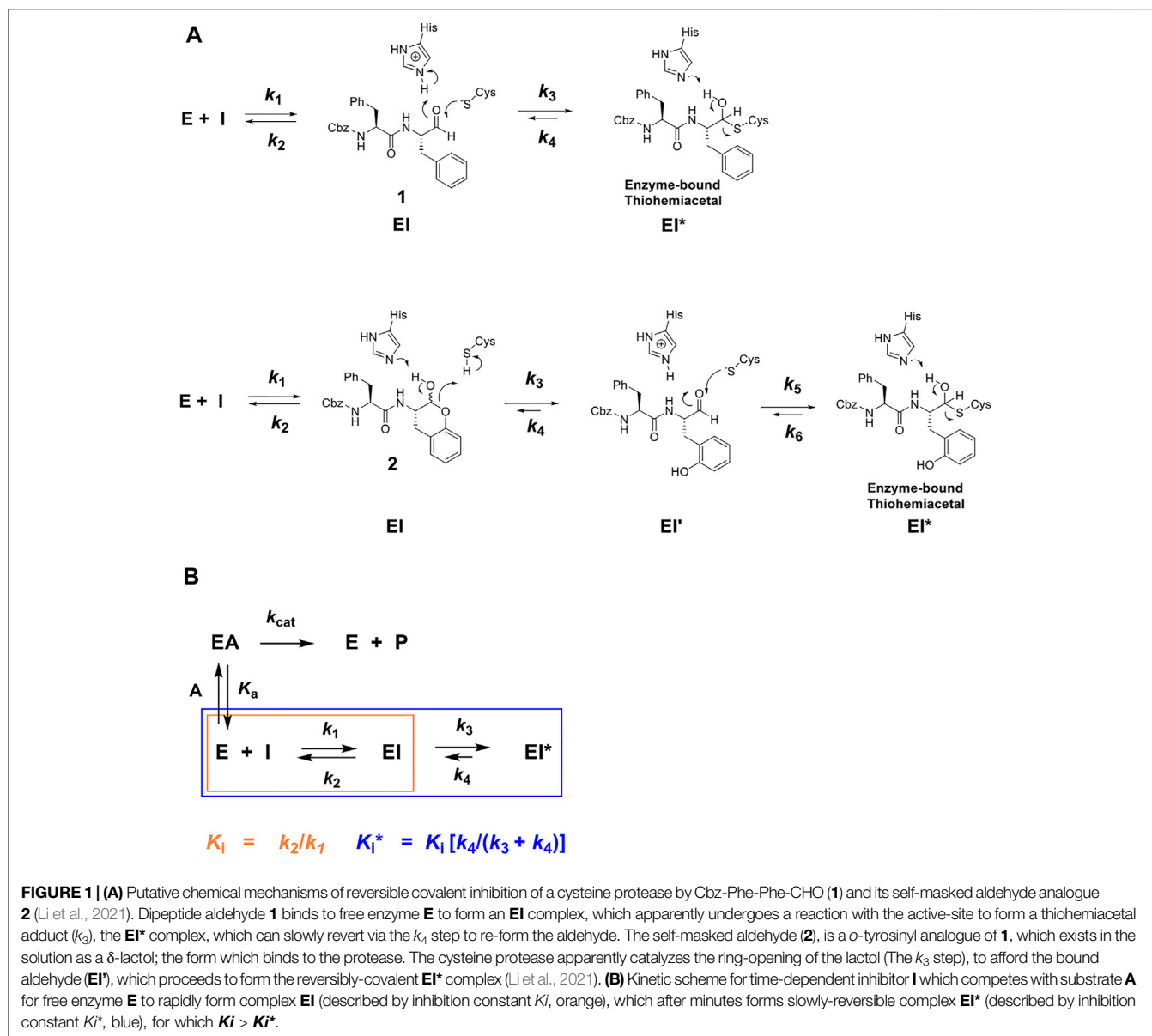
In general, the most effective inhibitors of cysteine proteases are peptide analogues bearing electrophilic warheads, which undergo reaction with the active-site cysteine (Puzer et al.,

2004; Cianni et al., 2019; and Cianni et al., 2021). The peptide or peptidomimetic moieties of such inhibitors are based on the substrate specificity of the target cysteine protease, and are therefore designed to selectively guide the appended warhead to the active-site of intent.

In this regard, the preferred peptide substrates of the cysteine protease cathepsin L (Brömmle et al., 1994; Puzer et al., 2004) and cruzain (Zhai and Meek, 2018) contain leucine, phenylalanine, or a similar amino-acid sidechain at the P_2 (Schechter and Berger, 1967) of the peptide, while for the CoV-2 3CL protease, a virtually invariant glutamine is found at the P_1 position, and leucine and other hydrophobic amino-acid sidechains exist at the P_2 positions (Rut et al., 2021). These preferences inform the development of specific peptide scaffolds for the inhibitors of these proteases. It is generally held that reversible covalent inhibition will afford inhibitors of higher selectivity and lower cytotoxicity than their irreversible counterparts, such as the vinyl sulfone warhead of **K777** (Doyle et al., 2007; Kerr et al., 2009). Peptide aldehydes comprise a long-standing class of reversible covalent inhibitors of the cysteine protease (Lewis and Wolfenden, 1977; Woo et al., 1995; Peheré et al., 2019).

In addition to the essentiality of the 3CL protease to establish cellular infection by SARS-CoV-2, host-cell proteases are also involved, catalyzing the peptidolysis of the coronaviral spike protein (S), which is required for cellular uptake and intracellular trafficking of the coronavirus (Mellott et al., 2021;





Hoffmann et al., 2020). Accordingly, these host proteases may also provide additional drug targets for SARS-CoV-2 infection. We recently reported that **K777**, or **K11777**, a di-peptide vinyl sulfone inactivator of the trypanosomal cysteine protease, cruzain (Scheme 1), which had been a clinical candidate for Chagas disease (McKerrow et al., 2009), was an exceptionally potent anti-SARS-CoV-2 agent (Mellott et al., 2021). We used a propargyl analogue of **K777** to covalently label and characterize the cellular target of **K777** in SARS-CoV-2-infected Vero E6 cells. We showed that cathepsin L was specifically labeled by **K777**, and in addition, we demonstrated that purified human cathepsin L catalyzed a unique cleavage of the spike protein from SARS-CoV-2; an event that assists the coronaviral uptake. As a result, human cathepsin L comprises an additional cellular target for the development of anti-COVID-19 agents.

While peptidic aldehydes form reversible thiohemiacetal adducts with the active-site cysteines of cysteine proteases (Cianni et al., 2021; Lewis and Wolfenden, 1977; Peheré et al., 2019; and Woo et al., 1995), and thereby afford exceptionally potent inhibition, free aldehydes are in general too reactive to provide therapeutic agents (Kaplowitz, 2005; Gampe and Verma, 2020; and O'Brien et al., 2005). However, CAT811, a macrocyclic aldehyde which is an inhibitor of the cysteine protease calpain, may be applied topically to the eye leading to the reduction of cataract formation (Morton et al., 2013). Consequently, we developed a novel class of reversible covalent inhibitors of cruzain, known as self-masked aldehyde inhibitors (SMAs). SMAs exist in aqueous solutions as stable δ -lactols, and in our hands, cruzain catalyzed the opening of the lactol to provide the enzyme-bound aldehyde, which subsequently

formed a thiohemiacetal adduct with cruzain (**Figure 1**) (Li et al., 2021). These SMAIs provided potent inhibition of cruzain ($K_i = 18\text{--}350$ nM), and some of these compounds demonstrated potent anti-trypanosomal activity in cellular-infection models of Chagas disease (Li et al., 2021). Given that human cathepsin L and cruzain share 36% amino-acid identity, and consequently, similar peptide-substrate specificity, we sought to characterize these SMAIs as inhibitors of human cathepsin L, and then evaluate potent inhibitors as potential anti-SARS-CoV-2 agents in models of cellular infection. We describe the results of these studies herein. In the preparation of this article, we became aware that benzyl δ -lactols of structures similar to our SMAIs are found in the anti-bacterial, nature-products known as cordycepamides (Fan et al., 2020).

MATERIALS AND METHODS

Chemicals

Sodium acetate, disodium-EDTA, Tris-HCl, and NaCl were obtained from Millipore Sigma. CHAPS and dithiothreitol were obtained from BioGold. Cbz-Phe-Arg-7-amino-4-methylcoumarin (Z-FR-AMC) was purchased from EMD Millipore or GenScript. The methods for the synthesis and characterization of the FRET-based substrate for 3CL-PR, (Abz)HN-Ser-Ala-Val-Leu-Gln*Ser-Gly-Phe-Arg-Lys (ϵ -Dnp)-CONH₂ is described in Mellott *et al.* (2021). The synthesis and characterization of all self-masked aldehyde inhibitors described in this work may be found in Li *et al.* (2021).

Cathepsins

Recombinant proteases were obtained from the following vendors: recombinant human cathepsin L (Millipore Sigma, Athens Research and Technology, Inc.), and human liver cathepsin B (Millipore Sigma), which were used without further purification. The solid proteins were dissolved into a solution of 50 mM sodium acetate (pH 5.5), 1 mM Na₂EDTA, 1 mM CHAPS, 10% (v/v) DMSO, and 5 mM DTT to final protein concentrations of 1–10 μ M in 20- μ L aliquots, and stored at -80°C until needed. These samples were then diluted into the same buffer to concentrations of ~ 100 nM, and these dilutions were stored at 4°C and used daily until depletion.

Expression and Purification of SARS-CoV-2 3CL Protease (3CL-PR)

The expression and purification of the 3CL-PR have been previously described (Mellott *et al.*, 2021). In brief, an expression construct of SARS-CoV-2 3CL-PR contained a GST domain at the N-terminus of the 3CL-PR coding sequence, followed by the 3CL-PR cleavage sequence (SAVLQ*SGF) preceding the sequence encoding the remaining 303 amino acids of the 3CL-PR monomer, followed at its C-terminus by a modified PreScission protease sequence (SGVTFQ*GP), that preceded a His₆ sequence (Zhang *et al.*, 2020; Mellott *et al.*, 2021). Upon expression, auto-proteolysis from 3CL-PR removed the N-terminal GST tag, yielding the authentic N-terminus (SGF).

After binding this processed protein to a nickel-NTA column, eluted fractions were pooled and dialyzed to remove imidazole. Proteolysis of the C-terminal H₆ tag was conducted by incubating with 3.5 units of HRV 3C Protease (Thermo Fisher Scientific) per mg of 3CL-PR (determined by Nanodrop) at 4°C overnight. Subsequently, the protein mixture was subjected to chromatography on a 5-ml GStrap HP column, and then a 5-ml HisTrap HP column (GE Healthcare), to remove, respectively, the GST-fused HRV 3C protease and undigested H₆-tagged protein. After chromatography on an anion exchange column and gel-filtration column, the tag-free 3CL-PR was pooled and concentrated (10 kDa molecular weight cutoff filter, GE Healthcare). The protein was deemed to be $\geq 95\%$ pure by SDS-PAGE, and was stored at -80°C in 12 mM Tris-HCl, 120 mM NaCl, 0.1 mM EDTA, and 2 mM DTT, (pH 7.5) with 50% glycerol (v/v). Analytical gel filtration indicated that native 3CL-PR was the expected homodimer (68 kDa).

Kinetic Assays and Characterization of Inhibition for Human Cathepsin B and L

For assays of cathepsin L and B, inhibitors were evaluated in 0.25-ml reaction mixtures containing a buffer of sodium acetate (pH 5.5), 1 mM CHAPS, 1 mM Na₂EDTA, and 5 mM DTT at 25°C . The fluorogenic substrate Cbz-Phe-Arg-7-amino-4-methylcoumarin (Z-FR-AMC) was dissolved in 100% DMSO, as were all inhibitors and aliquots of both substrates, and inhibitors were added to the reaction mixtures with final concentrations of DMSO of 10% (v/v). Reactions were initiated by addition of the proteases to final concentrations of 1–2 nM of either cathepsin L or cathepsin B. Michaelis constants for Z-FR-AMC were determined for cathepsin L ($K_m = 2.9$ μ M) and cathepsin B ($K_m = 150$ μ M), and fixed concentrations of Z-FR-AMC of 1x or 2x K_m were used to evaluate inhibitors. Formation of the fluorescent product AMC was monitored over 30–60-min time courses for reaction mixtures in 96-well black microplates (Greiner). Rates of peptidolysis of the dipeptide-AMC substrate(s) were measured on either a SpectraMax M2 (Molecular Devices) or a Synergy Mx (Biotek, Wisnooki, VT) microplate reader which measured the formation of fluorescence using an excitation wavelength of $\lambda_{ex} = 360$ nm, with detection of emission at $\lambda_{em} = 460$ nm at ≥ 8 -s intervals. Control samples excluded substrate. The measured relative fluorescence units (RFUs) of generated AMC were converted to reaction rates of $\mu\text{M/s}$ by use of a standard curve of known AMC concentrations obtained for both plate readers.

Kinetic Analysis of SARS-CoV-2 3CL-PR and Characterization of Its Inhibitors

In reaction mixtures containing 20 mM Tris-HCl (pH 7.5), 150 mM NaCl, 0.1 mM EDTA, 2 mM DTT, 10% (v/v) DMSO (a final concentration arising from addition of substrates and inhibitors added from 100% (v/v) DMSO solutions), and variable concentrations (10–175 μ M) of the FRET-based substrate Abz-SAVLQ*SGFRK (DNP)-NH₂,⁵ the reaction was initiated by the addition of 3CL-PR to final concentrations of 25–50 nM in 96-

well plates (Greiner, flat-bottom half volume, clear black plates). Rates of peptidolysis of the Abz-SAVLQ*SGFRK (DNP)-NH₂ substrate were measured on either a SpectraMax M5 (Molecular Devices) or a Synergy HTX (Biotek, Wisnooki, VT) microplate reader with $\lambda_{\text{ex}} = 320$ nm, $\lambda_{\text{em}} = 420$ nm in 8–60 s intervals, and time courses of inhibition were obtained for either 30 or 60 min intervals. Control samples excluded the substrate. The measured relative fluorescence units (RFUs) of the generated Abz-SAVLQ-COOH were converted to reaction rates of $\mu\text{M/s}$ by use of a standard curve of known concentration of fully hydrolyzed substrates obtained for both plate readers.

Cell Culture and Evaluation of Efficacy in SARS-CoV-2 Infection

Vero E6 cells [CRL:1586, ATCC], derived from African green monkey cells were grown in an Eagle's minimal essential medium (EMEM) supplemented with standard doses of penicillin and streptomycin, and 10% fetal bovine serum (FBS), which we designate as the M-10 medium. Human A549 cells that had been stably transduced with human ACE2 viral receptor (A549/ACE2), and then selected for increased ACE2 receptor, were grown in M-10. SARS-CoV-2 (USA_WA1/2020 isolate), the 3rd passage in Vero E6 cells from the original CDC (Atlanta) material with a confirmed sequence, was used throughout the study. A modified Vero E6-based standard micro-neutralization assay was used to rapidly evaluate the drug efficacy against the SARS-CoV-2 infection. Briefly, confluent Vero E6 or A549/ACE2 cells grown in 96-wells microtiter plates were pre-treated with 78 nM to 20 μM of the SMAIs and K777 (2-fold serially diluted) for 2 h, before infection with ~ 100 or ~ 500 infectious SARS-CoV-2 particles, respectively, in 100 μL EMEM supplemented with 2% FBS (2-MEM). Cells pre-treated with 2-fold serially-diluted dimethyl sulfoxide (DMSO; final concentration = 1% (v/v)) with or without the virus were included as positive and negative controls, respectively. After cultivation at 37°C for 3 days (Vero E6) or 4 days (A549/ACE2), individual wells were observed by microscopy for the status of a virus-induced formation of the cytopathic effect (CPE). The efficacy of individual drugs was calculated and expressed as the lowest concentration capable of completely preventing virus-induced CPE in 100% of the wells. The values of EC₅₀ (the concentration of inhibitor that results in a 50% growth of the virus) were determined in two ways: 1) In duplicate samples of a single compound dilution in which 100% CPE was observed for both replicates, and in which no CPE was observed at the next highest concentration of the inhibitor in duplicates, we assigned the value of EC₅₀ as the average of these two concentrations. 2) In cases in which duplicate concentrations result in one sample displaying CPE while the other does not, the value of EC₅₀ was assigned to this concentration. All experiments using infectious viruses were conducted at the University of Texas Medical Branch under BSL-3 conditions.

Fitting of Kinetic Data

The time-course data for compounds which exhibited time-dependent inhibition were fitted to **Eq. 1**, for which P is the relative fluorescence units of the AMC product, where v_i and v_s are the initial ($t < 500$ s) and steady-state ($t > 3,000$ s)

velocities, respectively, and k_{obs} is the rate constant of conversion of v_i to v_s , t is time in seconds, and C is a background constant.

$$P = v_s t + \left(\frac{v_i - v_s}{k_{\text{obs}}} \right) (1 - e^{-k_{\text{obs}} t}) + C \quad (1)$$

Resulting values of k_{obs} vs. $[I]$ were re-plotted and fitted to **Eq. 2**, in which k_3 and k_4 represent the respective rates of formation and reversion of the **EI*** complex as shown in **Figure 1B**, in which $K_i = k_2/k_1$ and $K_i^* = (k_2/k_1) (k_4/(k_3 + k_4))$, and for which A is the fixed substrate concentration, and K_a is the Michaelis constant.

$$k_{\text{obs}} = k_4 + \frac{k_3 [I]}{K_i \left(1 + \frac{[A]}{K_a} \right) + [I]} \quad (2)$$

Linearity of k_{obs} vs. $[I]$ of the inhibitor compounds will be observed when $K_i \gg K_i^*$. Under these conditions, the concentration of inhibitors required to observe time-dependent inhibition would be much less than the value of K_i for the **EI** complex. In this case, **Eq. 2** reduces to **Eq. 3**, which is a linear function with a slope = $k_3/[K_i (1 + [A]/K_a)]$ and a y -intercept = k_4 .

$$k_{\text{obs}} = k_4 + \frac{k_3 [I]}{K_i \left(1 + \frac{[A]}{K_a} \right)} \quad (3)$$

Inhibition constants (K_i and K_i^* values) were also obtained by fitting plots of v_i/v_0 and v_s/v_0 vs. $[I]$ to **Eqs 4** and **5**, wherein v_i and v_s are velocities at the early and late stages of the time courses of inhibition, respectively, v_0 is v_i and v_s when no inhibitor is present, $[I]$ is variable concentrations of the inhibitor, and K_a is the Michaelis constant of the substrate.

$$\frac{v_i}{v_0} = \frac{1}{\left\{ 1 + \frac{[I]}{K_i \left(1 + \frac{[A]}{K_a} \right)} \right\}} \quad (4)$$

$$\frac{v_s}{v_0} = \frac{1}{\left\{ 1 + \frac{[I]}{K_i^* \left(1 + \frac{[A]}{K_a} \right)} \right\}} \quad (5)$$

RESULTS AND DISCUSSION

Inhibition of Cysteine Proteases

The time courses of the inhibition of human cathepsin L by the parent aldehyde inhibitor in this study, Cbz-Phe-Phe-CHO (**1**), demonstrated initial inhibition, arising from the immediate formation of an **EI** complex, that apparently isomerized to a tighter complex (**EI***) in a concentration-dependent manner, after 1,000 s of incubation (**Figures 1, 2A**), in a manner nearly indistinguishable from that observed for cruzain (Li et al., 2021). By fitting the time course at each concentration of **1** to **Eq. 1**, we obtained values of k_{obs} , v_i , and v_s ; the latter two of which were normalized by the division of each value by the corresponding value of v_i and v_s in which $[I] = 0$, to provide values of v_i/v_0 and v_s/v_0 . A replot of the values of k_{obs} vs. $[I]$ (**Figure 2A**, inset) were fitted to both **Eqs 2, 3**. The apparent lack of a hyperbolic response

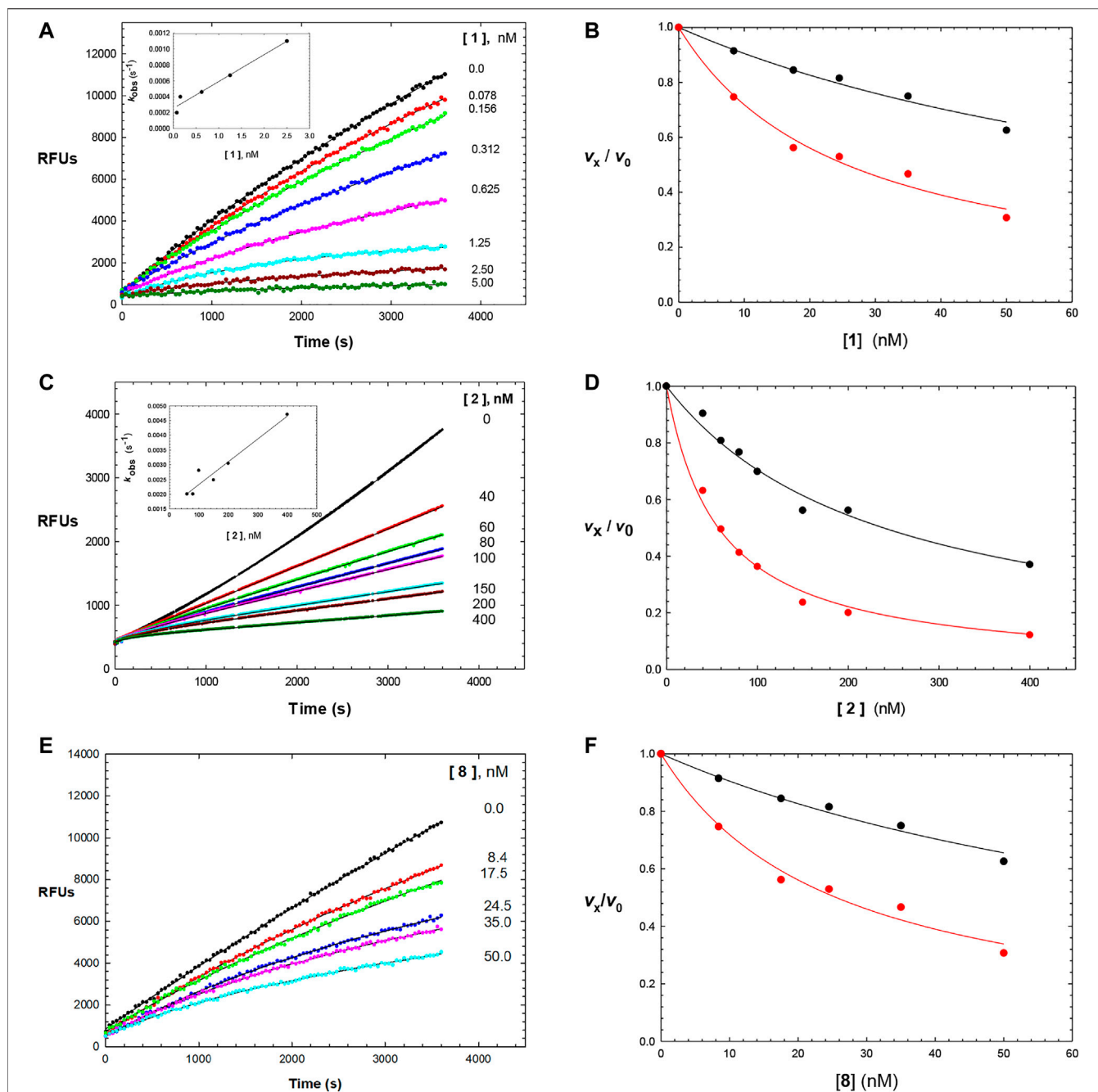


FIGURE 2 | Time courses (0–3600 s) of the inhibition of human cathepsin L by Cbz-Phe-Phe-CHO (**1**) (**A**); 0–5 nM of compound **1**, Cbz-Phe-o-Tyr-CHO (**2**) (**C**); 0–400 nM of compound **2**, and NMe-Pip-Phe-o-Tyr-CHO (**8**) (**E**); 0–50 nM of compound **8**. The measured RFUs (relative fluorescence units) were obtained upon cleavage of the fluorogenic peptide substrate Cbz-Phe-Arg-AMC (10 μ M; **3X** its apparent Michaelis constant with human cathepsin L). The lines drawn through the experimental points were from the plotting of each line to Eq. 1, and resulting values of v_i and v_s were normalized by dividing by v_i and v_s at $[I] = 0$ (v_0), to provide values of v_i/v_0 and v_s/v_0 , which were then replotted vs. each concentration of inhibitor as v_i/v_0 vs. [inhibitor] (black) and v_s/v_0 vs. [inhibitor] (red) in (**B,D,F**). Each plot was fitted to versions of the Cheng–Prusoff equation (Eq. 4 for v_i/v_0 , and Eq. 5 for v_s/v_0), to provide, the apparent inhibition constants of K_i and K_i^* , respectively. The insets in Figures 2A,C are replots of k_{obs} vs. [1] and k_{obs} vs. [2], from values of k_{obs} obtained from each time-course curve for each inhibitor from fitting to Eq. 1, respectively. The line drawn through the inset plots were from fitting to Eq. 3, resulting in values of $k_3/[K_i(1 + [A]/K_a)] = (1.5 \pm 0.2) \times 10^{-4} \text{ nM}^{-1} \text{ s}^{-1}$ and $k_4 = (2.6 \pm 0.5) \times 10^{-4} \text{ s}^{-1}$ (inhibitor **1**), and $k_3/K_i = (4 \pm 0.5) \times 10^{-6} \text{ nM}^{-1} \text{ s}^{-1}$ and $k_4 = 0.0016 \pm 0.0002 \text{ s}^{-1}$ (inhibitor **2**). Fitting of v_i/v_0 and v_s/v_0 vs. [8] resulted in values of K_i and K_i^* which are found in Table 1, along with all inhibition parameters.

of k_{obs} by **1** indicated that K_i was much greater than the applied concentrations of the aldehyde, and that Eq. 3 was the more appropriate equation for data fitting. Consequently, the use of Eq.

3 resulted in values of $k_3/[K_i(1 + [A]/K_a)] = (1.5 \pm 0.2) \times 10^{-4} \text{ nM}^{-1} \text{ s}^{-1}$ and $k_4 = (2.6 \pm 0.5) \times 10^{-4} \text{ s}^{-1}$, from which we may calculate $k_4K_i/k_3 \sim K_i^* = 13 \text{ nM}$. The rate constant for the

TABLE 1 | Self-masked aldehyde inhibitors of cysteine proteases and their effects on SARS-CoV-2 infected cells^a.

Compound	R ₄	R ₃	R ₂	R ₁ -A	K _i * (nM)				Anti-CoV-2 EC ₅₀ (μM)	
					hCatL	Cruzain ^b	hCatB	3CLpro ^b	Vero E6 Cells	A549/ACE2 Cells
1	H		Bz		0.14 ± 0.01	0.44 ± 0.02	ND	>10,000	0.47/7.5	>20
2	H	Cbz	Bz		12.6 ± 0.4	49 ± 2	4,500 ± 100	>10,000	10 ± 5	>20
3	OMe	Cbz	Bz	o-Tyr-CHO	17 ± 0.9	350 ± 30	5,500 ± 400	>10,000	ND	ND
4	Me	Cbz	Bz	o-Tyr-CHO	26 ± 0.9	103 ± 5	6,100 ± 900	>10,000	ND	ND
5	Cl	Cbz	Bz	o-Tyr-CHO	12.1 ± 0.3	70 ± 10	1400 ± 100	>10,000	ND	ND
6	F	Cbz	Bz	o-Tyr-CHO	10.3 ± 0.5	48 ± 2	2,300 ± 200	>10,000	4	ND
7	CO ₂ Me	Cbz	Bz	o-Tyr-CHO	4.8 ± 0.2	18.0 ± 0.5	670 ± 30	>10,000	2.5	ND
8	H		Bz	o-Tyr-CHO	9.0 ± 0.4	47 ± 2	1270 ± 70	>10,000	9 ± 2	ND
9	H				22 ± 4	ND	ND	9 ± 2 ^b	ND	3.75
10	H	Me-Pip	Bz		NA	NA	NA	NA	2.5	0.31
11	H	Me-Pip	Bz		NA	NA	NA	NA	2.5	0.62
12	H	Me-Pip	Bz		NA	NA	NA	NA	4	0.31
K777 ^c	NA	Me-Pip			k _{inact} /K _i = 3 ± 1 μM ⁻¹ ·s ⁻¹	k _{inact} /K _i = 1.0 ± 0.3 μM ⁻¹ ·s ⁻¹	k _{inact} /K _i = 0.009 ± 0.004 μM ⁻¹ ·s ⁻¹	>10,000	0.62 ^c / 0.15	<0.078 ^c
PF-07321332					>100mM ^d	ND	>100mM ^d	3.11 ^d	0.074 ^d / >20	0.077 ^d / 0.47

^aInhibition constants (K_i* values) obtained after 30-min incubation of inhibitors with cysteine proteases as described in Methods.

^bData for human cathepsins B and L were obtained at pH 5.5, and at neutral pH for cruzain (pH 7.5) (Zhai and Meek, 2018) and for 3CL protease (pH 7.2).

^cKinetic parameters of inactivation for K777 are as reported in Mellott et al. (2021).

^dData from Owen et al. (2021); NA, not applicable; ND, no data.

reversal of the EI* complex to EI is exceptionally slow ($k_4 = (2.6 \pm 0.5) \times 10^{-4} \text{ s}^{-1}$), and this is an important factor in the observed, sub-nanomolar value of K_i*, and also reflects the apparent stability of the enzyme-thiohemiacetal complex of EI*. Fitting

of the plots of v_i/v_0 and v_s/v_0 vs. [I], Eqs. 4 and 5, resulted in respective inhibition constants of $K_i = 0.18 \pm 0.22 \text{ nM}$ and $K_i^* = 0.14 \pm 0.01 \text{ nM}$ (Figure 2B), respectively, demonstrating that Cbz-Phe-Phe-CHO is an exceptionally potent inhibitor of human

cathepsin L (**Table 1** and **Figure 2A**), and is 3-fold more potent than its inhibition of cruzain ($K_i^* = 0.44 \pm 0.04$ nM (Li et al., 2021), **Table 1**).

Its analogue, the self-masked aldehyde Cbz-Phe-*o*-Tyr-CHO (**2**) demonstrated less time-dependent inhibition compared to **1** (**Figure 2C**), and again, the replot of k_{obs} vs. [**2**] (**Figure 2C**, inset) was linear. Fitting of these data to **Eq. (3)** resulted in the values of $k_3/K_i = (8 \pm 1) \times 10^{-6}$ nM⁻¹ s⁻¹ and $k_4 = 0.0016 \pm 0.0002$ s⁻¹, leading to $k_4K_i/k_3 \sim K_i^* = 200$ nM. The conversion of the apparent EI* to EI (rate constant of $k_4 = 0.0016 \pm 0.0002$ s⁻¹) is ~5-fold faster than that of aldehyde **1**, which contributes to the 100-fold weaker inhibition of **2**, as exemplified by K_i^* (see below). As discussed in our study of compound **2** with cruzain, we ascribed this faster rate of reversion of the thiohemiacetal (EI* to EI) due to the facilitation of the phenoxide group of **2** to break the C–S bond of the thiohemiacetal to elicit reformation of the lactol of **2** (Li et al., 2021). Fitting of plots of v_i/v_0 and v_i/v_0 vs. [**2**] to, **Eqs 4** and **5**, resulted in respective inhibition constants of $K_i = 54 \pm 6$ nM and $K_i^* = 12.6 \pm 0.4$ nM. Also, as with cruzain, the self-masked aldehyde analogue of **1** (Cbz-Phe-*o*-Tyr-CHO (**2**)) was 100-fold less potent as an inhibitor of cathepsin L, but the value of K_i^* of **2** for cathepsin L was 3.9-fold more potent than that observed for cruzain (**Table 1**). The kinetic behavior of the inhibitors of **1** and **2** are very similar to that observed with cruzain (Li et al., 2021).

Addition of the electron-donating groups methoxy (**3**) and methyl (**4**) at the 4'-position of the *o*-Tyr group resulted in respective 1.4-fold and 2-fold increases in their K_i^* values compared to **2**, while the substitution of **2** at this position with the electron-withdrawing groups fluoro (**5**) and chloro (**6**) had little effect on the inhibition of cathepsin L compared to unsubstituted compound **2**. With the exception of compound **3**, these inhibitors were ≥ 2 -fold more potent for human cathepsin L than cruzain, which also indicated that substitution at the 4'-position had less of an effect on the inhibition of cathepsin L than that of cruzain. Like with cruzain, the 4'-methylcarboxylate substituent of compound **7** improved potency 2.6-fold over that of **2**, and afforded the most potent SMAI in this series of compounds. Substitution of the terminal Cbz group of **2** with an N-methyl-piperidinyl urea provided a more potent analogue of **2**: compound **8** (**Figures 2E and F**), for which values of $K_i = 22 \pm 1$ nM and $K_i^* = 9.0 \pm 0.4$ nM were obtained. Inhibitor **8** has greater aqueous solubility than **2** (Li et al., 2021), and was nearly twice as potent as **2** for human cathepsin L. In the earlier study, we showed that the [*aldehydic*-¹³C] form of compound **8**, as analyzed by ¹H-¹³C HSQC NMR, remained exclusively in its δ -lactol form in aqueous reaction buffer, but upon the addition of an equimolar amount of cruzain, changes to the chemical shifts in the NMR data were consistent with the formation of an enzyme-bound thiohemiacetal adduct (Li et al., 2021). The improved potency of compound **8** with cathepsin L suggests, but does not prove, that cathepsin L in kind, catalyzes the opening of the δ -lactol form leading to the formation of a thiohemiacetal with cathepsin L.

Where studied, the SMAIs in **Table 1** were 120–320-fold less potent inhibitors of human cathepsin B than with cathepsin L. This selectivity also underscores the 36% amino-acid identity between cruzain and human cathepsin L, while there is only a 29% amino-

acid identity between human cathepsins L and B. Expectantly, none of compounds **1–8** exhibited inhibition of the SARS-CoV-2 3CL protease at concentrations of 10 μ M or lower (**Table 1**).

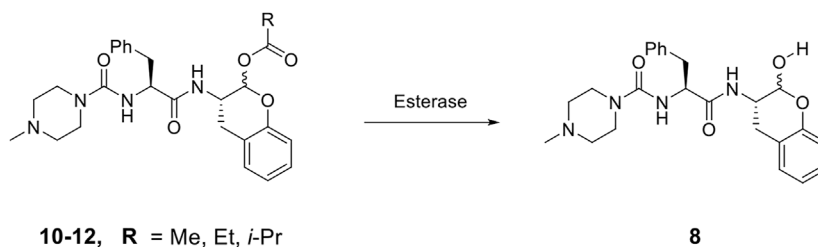
Modifications of SMAIs to Develop 3CL-PR Inhibitors That are Also Inhibitors of Human Cathepsin L

We sought to identify an amino-acid sidechain at the P₁ position of a peptide scaffold which would be recognized by both human cathepsin L and SARS-CoV-2 3CL PR. To date, only 2-oxopyrrolidinyl-alanyl groups (Op-Ala), in effect, glutaminyllactams, have afforded suitable sidechains at the P₁ position for inhibitors of SARS-CoV-2 3CL-PR (Dai et al., 2020; Zhang et al., 2020; and Owen et al., 2021). Given that the substituted or un-substituted phenylalanyl groups at the P₁ position within the peptidomimetic scaffolds of compounds **1–8** provide potent cathepsin L inhibitors that had no effect on purified 3CL protease, we sought to find an amino-acid group for the P₁ sidechain that would be accommodated by both human cathepsin L and SARS-CoV-2 3CL protease. Such bi-functional anti-CoV-2 agents would presage a novel class of COVID-19 drugs that might subvert the development of viral mutations that thwart the action of drugs that only target 3CL protease, or for that matter, cathepsin L.

We hypothesized that compound **9** would be an inhibitor of both 3CL protease and human cathepsin L. In this SMAI, the P₃ position contains a valyl group, the P₂ position contains the leucyl analogue cyclohexyl-alanyl, and the P₁ position contains the novel glutamine analogue, 2-pyridone (Li et al., 2021). We expected the 2-pyridone aldehyde to also form a δ -lactol, and also be recognized by both human cathepsin L and SARS-CoV-2 3CL protease, and this was indeed the case. Compound **9** is a low nanomolar inhibitor of both enzymes ($K_i = 22$ nM for human cathepsin L, and $K_i = 9$ nM for SARS-CoV-2 3CL protease), demonstrating the feasibility of designing an inhibitor to target both enzymes.

Prodrugs of SMAI 8

As compound **8**, an inhibitor with a peptidomimetic scaffold similar to that of the anti-chagasic compound **K777** (common elements include the P₃ N-methyl-piperazinoyl group and the P₂ phenylalanyl group), demonstrated potent inhibition of human cathepsin L, we sought to protect the δ -lactol functionality of **8** by synthesizing pro-drug forms in which the secondary alcohol of **8** was acylated. (Li et al., 2021) (**Scheme 2**). Compounds **10–12**, respectively comprise the O-acetyl, O-*n*-propanoyl, and the O-isobutanoyl derivatives of lactol **8**. We previously demonstrated that treatment of pro-drugs **10–12** with porcine esterase *in vitro* generated inhibitor **8** (**Scheme 1**). Pro-drugs **10–12** exerted anti-trypanosomal activity at micromolar concentrations in infected-cell cultures which was superior to that of the free lactol **8** (Li et al., 2021). From these results we sought to evaluate these pro-drug forms of **8**



SCHEME 2 | De-acylation of Pro-drugs of Compound 8 as catalyzed by cellular esterases.

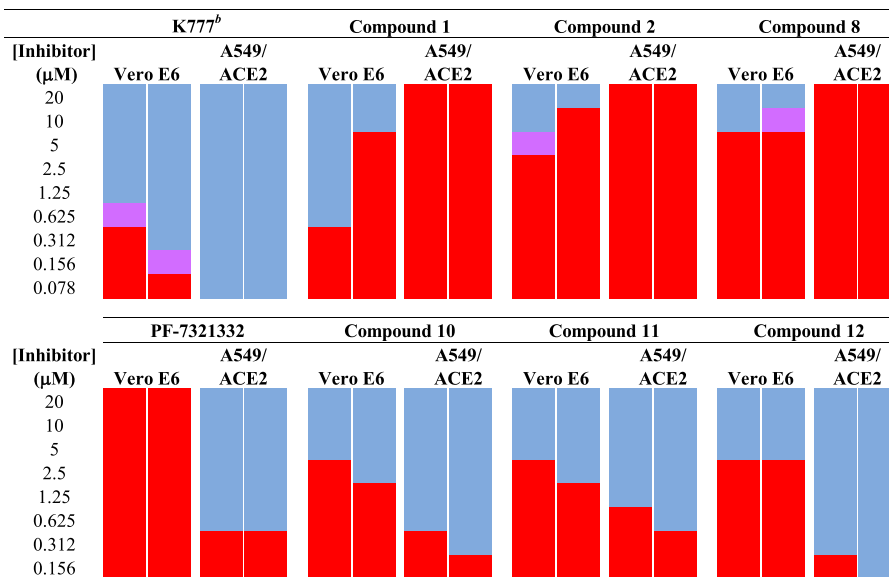


FIGURE 3 | Anti-SARS-CoV-2 activity of SMAIs, compared to that of **K777** and **PF-07321332**. SARS-CoV-2-infected Vero E6 and human A549/ACE2 cells were treated as described with **K777**, aldehyde **1**, SMAIs **2**, **8**, and the pro-drug forms of **8**, compounds **10-12**.

in SARS-CoV-2-infected mammalian cells, as described below.

Anti-SARS-CoV-2 Activities of the SMAIs

We tested aldehyde **1**, selected SMAIs (compounds **2**, **8**, **10-12**), and the approved drug **PF-07321332**, in two types of mammalian cells (Vero E6 and A549/ACE2) infected with SARS-CoV-2 (Figure 3 and Table 1), along with data for **K777** as previously reported (Mellott et al., 2021). Vero E6 are derived from African green monkeys, while A549/ACE2 cells are human adenocarcinoma cells that are stably transduced with the human ACE2 viral receptor. We previously found that **K777**, an irreversible inactivator of human cathepsin L blocked the SARS-CoV-2-induced cytopathic effect (CPE) in Vero E6 and A549/ACE2 cells at respective values of $EC_{50} = 625$ and <78 nM. In a second study, an EC_{50} of 156 nM was obtained in Vero E6 cells. These activities of **K777** are among the most potent yet observed for any inhibitor of SARS-CoV-2 cell infection. The anti-SARS-CoV-2 effects of **PF-07321332** in infected Vero and A549/ACE2 cells were reported as respective EC_{50} values of 74

and 77 nM. However, in our hands, **PF-07321332** had no anti-SARS-CoV-2 effects in Vero E6 cells at concentrations of ≤ 20 μ M, while we measured a value of $EC_{50} = 470$ nM in A549/ACE2 cells, which is >6 -fold less potent than **K777**. Regardless of the reasons for these differences obtained in two different laboratories, we consider the results we report in our studies to serve as “benchmark” data for an approved drug to compare with our inhibitors.

Dipeptide aldehyde **1** was a potent anti-SARS-CoV-2 agent in Vero E6 cells ($EC_{50} = 470$ nM), but upon repeating this experiment with a different sample of **1**, we observed a value of $EC_{50} = 7.5$ μ M. The cause of this discrepancy is unknown, as the experimental conditions are identical. Compound **1** exerted no inhibition of CPE in A549/ACE2 at concentrations of ≤ 20 μ M, which may validate the higher of the two EC_{50} values observed in Vero E6 cells. The value of EC_{50} for SMAI **2** was found to be 10 ± 5 μ M in Vero E6 cells, while in A549/ACE2 cells, there was no inhibition of CPE at concentrations of ≤ 20 μ M. The 4'-benzyl-substituted SMAIs **6** and **7** displayed a slightly higher anti-CoV-2 activity in Vero E6 cells, with respective values of $EC_{50} = 4$ and

2.5 μM in infected Vero E6 cells (**Table 1**). The more soluble SMAI, compound **8**, had a slightly increased anti-SARS-CoV-2 activity compared to SMAI **2** in Vero E6 ($\text{EC}_{50} = 9 \pm 2 \mu\text{M}$), but again, no anti-viral effect in infected A549/ACE2 cells. We previously reported (Li et al., 2021) that the dual inhibitor of human cathepsin L and 3CL-PR, compound **9**, had no effect in SARS-CoV-2-infected Vero E6 cells, but demonstrated an $\text{EC}_{50} = 3.75 \mu\text{M}$ in SARS-CoV-2-infected A549/ACE2 cells (**Table 1**).

Two of the three pro-drug analogues of compound **8**, compounds (**10–12**) proved the most potent anti-SARS-CoV-2 agents in our study. These inhibitors differ structurally from compound **8** only in that the secondary alcohol of the lactol of **8** is now O-acylated with, acetyl, propanoyl, and iso-butanoyl groups, respectively. As previously proposed (Li et al., 2021), we expected that O-acylation of this hydroxyl group would provide protection of the lactol from opening to the requisite aldehyde, and subsequent reaction with electrophiles within cells. Indeed, pro-drugs **10–12** were highly effective in preventing CPE in both Vero E6 (respective EC_{50} values of 2.5, 2.5, and 3.75 μM) and especially in A549/ACE2 cells (respective EC_{50} values of 312, 625, and 156 nM). It is notable that in A549/ACE2 cells, the more sterically-hindered O-iso-butanoyl group provided the most potent inhibition of CPE, suggesting that this ester has the highest metabolic stability in cells of the three pro-drugs studied. It is noteworthy that these three pro-drugs of SMAI **8** are effectively equipotent with that of **PF-07321332** in A549/ACE2 cells, and demonstrated an activity at low micromolar concentrations in CoV-2-infected Vero E6 cells, in which **PF-07321332** was inactive.

SUMMARY

In this report we have described the expanded use of our novel class of cysteine protease inhibitors, the self-masked aldehydes, to the inhibition of human cathepsin L, in which these inhibitors were more potent than their inhibition of the highly similar cysteine protease, cruzain, from the parasitic protozoan *Trypanosoma cruzi*. While none of the SMAIs inhibited the 3CL protease of SARS-CoV-2, some nevertheless demonstrated inhibition of the cytopathic effect arising from SARS-CoV-2 infection of two mammalian cell lines. SMAI **8** exhibited a value of $K_i = 9 \text{ nM}$ vs. human cathepsin L, but with moderate anti-SARS-CoV-2 activity at micromolar concentrations in Vero E6 cells, and with no

effect in the SARS-CoV-2-infected A549/ACE2 cells. However, three O-acylated pro-drug forms of **8** blocked CoV-2-mediated CPE in infected A549/ACE2 cells with potencies equivalent to that of the FDA-approved, 3CL-PR inhibitor **PF-07321332**. As we have embarked on the discovery of a single SMAI that inhibits both hCatL and SARS-CoV-2 3CL protease, as exemplified here by the 2-pyridone analogue of alanine compound **9**, which, while a nanomolar inhibitor of both enzymes, the anti-CoV-2 effects of this dual inhibitor are no better than that of SMAIs discussed previously. However, based on the success of pro-drug forms of human cathepsin L inhibitor **8**, it would be circumspect to synthesize O-acylated analogues of SMAI **9**, and evaluate them in cellular models of the SARS-CoV-2 infection. This will be the focus of upcoming studies.

DATA AVAILABILITY STATEMENT

The raw data supporting the conclusion of this article will be made available by the authors, without undue reservation.

AUTHOR CONTRIBUTIONS

Compounds were prepared and analyzed by LL and BC. 3CL protease was expressed and purified by AK, ZT, and DM, with support from FR. The FRET-based peptide for 3CL protease was prepared by DM or JZ. Inhibition kinetics was performed by JZ and LL, with assistance from CG, AD, VT, and C-TT provided SARS-CoV-2-cell infectivity data. TM wrote the manuscript. LL and JZ are co-first authors of this work.

FUNDING

Financial support for the research was provided by NIH grants R21 AI127634, R01 GM129076, and Texas A&M AgriLife Research.

ACKNOWLEDGMENTS

We thank Prof. Frank M. Raushel for supporting this work. We also thank Hayley Boswell for assistance with acquiring data.

REFERENCES

- Bai, B., Arutyunova, E., Khan, M. B., Lu, J., Joyce, M. A., Saffran, H. A., et al. (2021). Peptidomimetic Nitrile Warheads as SARS-CoV-2 3CL Protease Inhibitors. *RSC Med. Chem.* 12, 1722–1730. doi:10.1039/d1md00247c
- Brömme, D., Bonneau, P. R., Lachance, P., and Storer, A. C. (1994). Engineering the S2 Subsite Specificity of Human Cathepsin S to a Cathepsin L- and Cathepsin B-like Specificity. *J. Biol. Chem.* 269, 30238–30242. doi:10.1016/s0021-9258(18)43803-3
- Cianni, L., Rocho, F. D. R., Bonatto, V., Martins, F. C. P., Lameira, J., Leitão, A., et al. (2021). Design, Synthesis and Stepwise Optimization of Nitrile-Based Inhibitors of Cathepsins B and L. *Bioorg. Med. Chem.* 29, 115827. doi:10.1016/j.bmc.2020.115827
- Cianni, L., Feldmann, C. W., Gilberg, E., Gütschow, M., Juliano, L., Leitão, A., et al. (2019). Can Cysteine Protease Cross-Class Inhibitors Achieve Selectivity? *J. Med. Chem.* 62, 10497–10525. doi:10.1021/acs.jmedchem.9b00683
- Dai, W., Zhang, B., Jiang, X.-M., Su, H., Li, J., Zhao, Y., et al. (2020). Structure-based Design of Antiviral Drug Candidates Targeting the SARS-CoV-2 Main Protease. *Science* 368, 1331–1335. doi:10.1126/science.abb4489
- Doyle, P. S., Zhou, Y. M., Engel, J. C., and McKerrow, J. H. (2007). A Cysteine Protease Inhibitor Cures Chagas' Disease in an Immunodeficient-Mouse Model

- of Infection. *Antimicrob. Agents Chemother.* 51, 3932–3939. doi:10.1128/aac.00436-07
- Fan, W., Li, E., Ren, J., Wang, W., Liu, X., and Zhang, Y. (2020). Cordycepamides A–E and Cordyglycoside A, New Alkaloidal and Glycoside Metabolites from the Entomopathogenic Fungus *Cordyceps* Sp. *Fitoterapia* 142, 104525. doi:10.1016/j.fitote.2020.104525
- Gampe, C., and Verma, V. A. (2020). Curse or Cure? A Perspective on the Developability of Aldehydes as Active Pharmaceutical Ingredients. *J. Med. Chem.* 63, 14357–14381. doi:10.1021/acs.jmedchem.0c01177
- Hoffmann, M., Kleine-Weber, H., Schroeder, S., Krüger, N., Herrler, T., Erichsen, S., et al. (2020). SARS-CoV-2 Cell Entry Depends on ACE2 and TMPRSS2 and Is Blocked by a Clinically Proven Protease Inhibitor. *Cell* 181, 271–280. doi:10.1016/j.cell.2020.02.052
- Johns Hopkins University of Medicine. Coronavirus Resource Center. 2022. <https://coronavirus.jhu.edu/>.
- Kaplowitz, N. (2005). Idiosyncratic Drug Hepatotoxicity. *Nat. Rev. Drug Discov.* 4, 489–499. doi:10.1038/nrd1750
- Kerr, I. D., Lee, J. H., Farady, C. J., Marion, R., Rickert, M., Sajid, M., et al. (2009). Vinyl Sulfones as Antiparasitic Agents and a Structural Basis for Drug Design. *J. Biol. Chem.* 284, 25697–25703. doi:10.1074/jbc.m109.014340
- Lewis, C. A., Jr, and Wolfenden, R. (1977). Thiohemiacetal Formation by Inhibitory Aldehydes at the Active Site of Papain. *Biochemistry* 16, 4890–4895. doi:10.1021/bi00641a023
- Li, L., Chenna, B. C., Yang, K. S., Cole, T. R., Goodall, Z. T., Giardini, M., et al. (2021). Self-masked Aldehyde Inhibitors: A Novel Strategy for Inhibiting Cysteine Proteases. *J. Med. Chem.* 64, 11267–11287. doi:10.1021/acs.jmedchem.1c00628
- McKerrow, J. H., Doyle, P. S., Engel, J. C., Podust, L. M., Robertson, S. A., Ferreira, R., et al. (2009). Two Approaches to Discovering and Developing New Drugs for Chagas Disease. *Mem. Inst. Oswaldo Cruz.* 104 Suppl 1 (Suppl. 1), 263–269. doi:10.1590/s0074-02762009000900034
- Mellott, D. M., Tseng, C.-T., Drelich, A., Fajtová, P., Chenna, B. C., Kostomiris, D. H., et al. (2021). A Clinical-Stage Cysteine Protease Inhibitor Blocks SARS-CoV-2 Infection of Human and Monkey Cells. *ACS Chem. Biol.* 16, 642–650. doi:10.1021/acscchembio.0c00875
- Morton, J. D., Lee, H. Y. Y., McDermott, J. D., Robertson, L. J. G., Bickerstaffe, R., Jones, M. A., et al. (2013). A Macrocyclic Calpain Inhibitor Slows the Development of Inherited Cortical Cataracts in a Sheep Model. *Invest. Ophthalmol. Vis. Sci.* 54, 389–395. doi:10.1167/iovs.12-11088
- O'Brien, P. J., Siraki, A. G., and Shangari, N. (2005). Aldehyde Sources, Metabolism, Molecular Toxicity Mechanisms, and Possible Effects on Human Health. *Crit. Rev. Toxicol.* 35, 609–662. doi:10.1080/10408440591002183
- Owen, D. R., Allerton, C. M. N., Anderson, A. S., Aschenbrenner, L., Avery, M., Berritt, S., et al. (2021). An Oral SARS-CoV-2 M Pro Inhibitor Clinical Candidate for the Treatment of COVID-19. *Science* 374, 1586–1593. doi:10.1126/science.abl4784
- Peheré, A. D., Nguyen, S., Garlick, S. K., Wilson, D. W., Hudson, I., Sykes, M. J., et al. (2019). Tripeptide Analogues of MG132 as Protease Inhibitors. *Bioorg. Med. Chem.* 27, 436–441. doi:10.1016/j.bmc.2018.12.022
- Pfizer. *Pfizer Receives U.S. FDA Emergency Use Authorization for Novel COVID-19 Oral Antiviral Treatment*. Washington, DC: FDA Announcement. 2021. Retrieved 22 December 2021.
- Puzer, L., Cotrin, S. S., Alves, M. F. M., Egborge, T., Araújo, M. S., Juliano, M. A., et al. (2004). Comparative Substrate Specificity Analysis of Recombinant Human Cathepsin V and Cathepsin L. *Arch. Biochem. Biophys.* 430, 274–283. doi:10.1016/j.abb.2004.07.006
- Rut, W., Groborz, K., Zhang, L., Sun, X., Zmudzinski, M., Pawlik, B., et al. (2021). SARS-CoV-2 Mpro Inhibitors and Activity-Based Probes for Patient-Sample Imaging. *Nat. Chem. Biol.* 17, 222–228. doi:10.1038/s41589-020-00689-z
- Schechter, I., and Berger, A. (1967). On the Size of the Active Site in Proteases. I. Papain. *Biochem. Biophysical Res. Commun.* 27, 157–162. doi:10.1016/s0006-291x(67)80055-x
- Woo, J.-T., Sigeizumi, S., Yamaguchi, K., Sugimoto, K., Kobori, T., Tsuji, T., et al. (1995). Peptidyl Aldehyde Derivatives as Potent and Selective Inhibitors of Cathepsin L. *Bioorg. Med. Chem. Lett.* 5, 1501–1504. doi:10.1016/0960-894x(95)00236-m
- Zhai, X., and Meek, T. D. (2018). Catalytic Mechanism of Cruzain from *Trypanosoma Cruzi* as Determined from Solvent Kinetic Isotope Effects of Steady-State and Pre-steady-state Kinetics. *Biochemistry* 57, 3176–3190. doi:10.1021/acs.biochem.7b01250
- Zhang, L., Lin, D., Sun, X., Curth, U., Drosten, C., Sauerhering, L., et al. (2020). Crystal Structure of SARS-CoV-2 Main Protease Provides a Basis for Design of Improved α -ketoamide Inhibitors. *Science* 368, 409–412. doi:10.1126/science.abb3405

Conflict of Interest: The authors declare that the research was conducted in the absence of any commercial or financial relationships that could be construed as a potential conflict of interest.

Publisher's Note: All claims expressed in this article are solely those of the authors and do not necessarily represent those of their affiliated organizations, or those of the publisher, the editors, and the reviewers. Any product that may be evaluated in this article, or claim that may be made by its manufacturer, is not guaranteed or endorsed by the publisher.

Copyright © 2022 Zhu, Li, Drelich, Chenna, Mellott, Taylor, Tat, Garcia, Katzfuss, Tseng and Meek. This is an open-access article distributed under the terms of the Creative Commons Attribution License (CC BY). The use, distribution or reproduction in other forums is permitted, provided the original author(s) and the copyright owner(s) are credited and that the original publication in this journal is cited, in accordance with accepted academic practice. No use, distribution or reproduction is permitted which does not comply with these terms.